Earth and Planetary Science Letters 303 (2011) 215–224

Contents lists available at ScienceDirect

Earth and Planetary Science Letters

journal homepage: www.elsevier.com/locate/epsl

Diverse mantle sources for Ninetyeast Ridge magmatism: Geochemical constraints from basaltic glasses

F.A. Frey [a,*], M. Pringle [a], P. Meleney [a], S. Huang [b], A. Piotrowski [a]

[a] Department of Earth, Atmospheric and Planetary Sciences, Massachusetts Institute of Technology, Cambridge, MA 02139, United States
[b] Department of Earth and Planetary Sciences, Harvard University, Cambridge, MA 02138, United States

ARTICLE INFO

Article history:
Received 3 August 2010
Received in revised form 27 December 2010
Accepted 28 December 2010

Editor: R.W. Carlson

Keywords:
basaltic glass
Kerguelen
Ninetyeast Ridge
hotspot
ocean island basalt petrogenesis
mantle heterogeneity

ABSTRACT

The Ninetyeast Ridge (NER), a north–south striking, 5,000 km long, 77 to 43 Ma chain of basaltic submarine volcanoes in the eastern Indian Ocean formed as a hotspot track created by rapid northward migration of the Indian Plate over the Kerguelen hotspot. Based on the major and trace element contents of unaltered basaltic glasses from six locations along the NER, we show that the NER was constructed by basaltic magma derived from at least three geochemically distinct mantle sources: (1) a source enriched in highly incompatible elements relative to primitive mantle like the source of the 29–24 Ma flood basalts in the Kerguelen Archipelago; (2) an incompatible element-depleted source similar to the source of Mid-Ocean Ridge Basalt (MORB) erupted along the currently active Southeast Indian Ridge (SEIR); and (3) an incompatible element-depleted source that is compositionally and mineralogically distinct from the source of SEIR MORB. Specifically, this depleted mantle source was garnet-bearing and had higher Y/Dy and Nb/Zr, but lower Zr/Sm, than the SEIR MORB source. We infer that this third source formed as a garnet-bearing residue created during a previous melting event, perhaps an initial partial melting of the mantle hotspot. Subsequently, this residue partially melted over a large pressure range, from slightly over 3 GPa to less than 1 GPa, and to a high extent (~30%) thereby creating relatively high SiO_2 and FeO contents in some NER basalts relative to SEIR MORB.

1. Introduction

The Ninetyeast Ridge (NER) in the eastern Indian Ocean is a chain of volcanoes forming the longest volcanic lineament on earth; it strikes from 31°S to 10°N, where it is buried beneath sediments of the Bengal Fan. Recent Ar–Ar geochronology establishes a north to south decrease in eruption age, from 77 Ma at 5°N to 43 Ma at 31°S (Pringle et al., 2008; Fig. 1a). This observed age progression is remarkably linear, and consistent with the rapid northward migration of the Indian plate over a relatively fixed magma source, the Kerguelen hotspot, at a rate of 118 ± 5 km/my. Our objective is to use the major and trace element compositions of glasses, primarily from pillow lavas and breccia clasts dredged from the NER, to constrain the petrogenesis of magmas forming the NER and the relative roles of hotspot- and spreading ridge-derived magmas in forming NER volcanoes.

2. Samples studied

2.1. Sampling the Ninetyeast Ridge

The basaltic basement of the NER has been sampled at 7 Deep Sea Drilling Project (DSDP) and Ocean Drilling Program (ODP) drill sites and by dredging. The most comprehensive dredging effort was the 2007 KNOX06 cruise of the R/V Revelle, which recovered basalt at 23 dredge sites (Fig. 1).

Geochemical studies of whole-rocks from these NER drill cores and dredges show that the basement forming the upper part of NER volcanoes is dominantly tholeiitic basalt and less commonly alkalic basalt; both exhibit the relative enrichment in incompatible trace elements typical of ocean island basalt. In detail, most of the previously studied NER basalts have incompatible element abundances and Sr, Nd, and Pb isotopic ratios similar to lavas erupted in the Kerguelen Archipelago (Frey and Weis, 1995; Frey et al., 1991, 2008; Nobre Silva et al., 2008; Saunders et al., 1991; Weis and Frey, 1991).

2.2. Submarine volcanism on the NER

Most of the basaltic basement recovered by drilling along the NER was erupted subaerially; only 1 of the 7 drill sites recovered submarine erupted basalt (Frey and Weis, 1995; Frey et al., 1991; Saunders et al., 1991; Thompson et al., 1974). At ODP Leg 121 Drill Site 758, water depth of 2924 m, the northernmost sampling site on the NER (Fig. 1), the lowermost samples of the recovered 119 m of tholeiitic basalt core include submarine erupted sheet flows and pillow basalts. No fresh glasses from this core have been identified, but the whole-rocks have higher MgO contents (8 to 10%) than basalts

* Corresponding author. Tel.: +1 617 253 2818; fax: +1 617 253 7102.
E-mail address: fafrey@mit.edu (F.A. Frey).

0012-821X/$ – see front matter © 2011 Elsevier B.V. All rights reserved.
doi:10.1016/j.epsl.2010.12.051

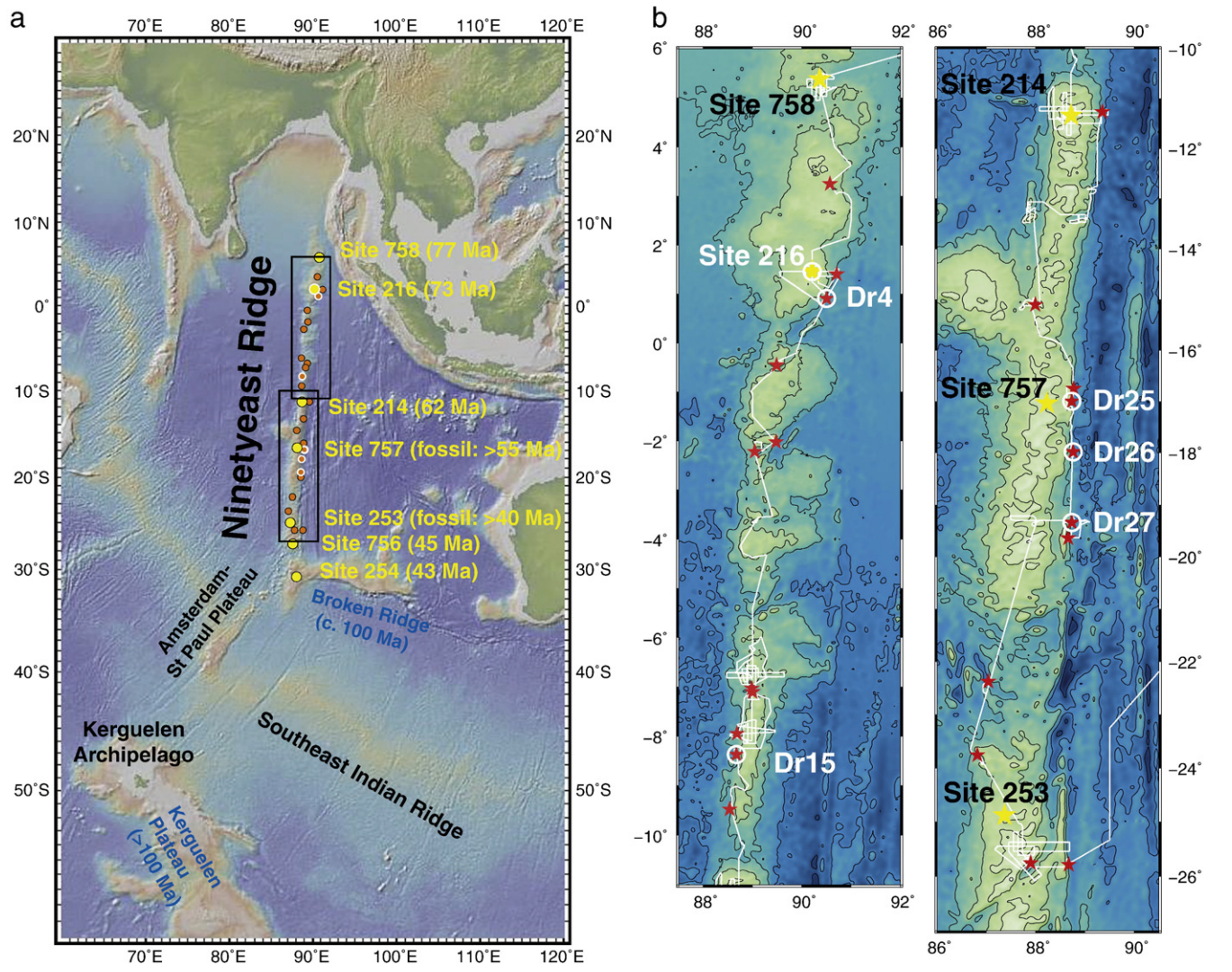

Fig. 1. a. Bathymetry of Eastern Indian Ocean seafloor. Major volcanic structures are labeled. Kerguelen Plateau and Archipelago, Southeast Indian Ridge (SEIR); Amsterdam–St.Paul (ASP) Plateau; the Amsterdam and St. Paul Islands are located near the SEIR-ASP Plateau intersection; Broken Ridge, which was conjugate with the Kerguelen Plateau prior to SEIR formation; and the Ninetyeast Ridge (NER). Detailed bathymetry of regions designated by rectangles is shown in Fig. 1b. Previous DSDP and ODP Drill Sites (yellow circles) are shown with 2007 R/V Roger Revelle-KNOX06 dredge locations (red and orange circles). Ar–Ar ages for NER basalt from previous DSDP and ODP Drill Sites and from 2007 R/V Roger Revelle KNOX06 samples (red circles) are consistent with a linear, north to south age progression of 118 ± 5 km/my (Pringle et al., 2008) from 77 to 43 Ma. This trend is consistent with the NER having formed as a hotspot track related to the Kerguelen hotspot. b. Bathymetry of the NER under the 2007 R/V Roger Revelle KNOX06 cruise ship track. Dredge locations indicated with red stars; yellow stars indicate DSDP and ODP drill sites which recovered basalt. Dredges that contain fresh basaltic glass are labeled and circled in white. Contour interval: 1000 m.

recovered from other NER drill sites; hence these submarine erupted samples have experienced less post-melting processing than most subaerially erupted NER magmas. Based on incompatible trace element abundances and Sr and Nd isotopic ratios, Site 758 basalts are mixtures of hotspot-derived magmas with a large proportion of magma derived from a MORB source (Frey et al., 1991; Weis and Frey, 1991).

Basaltic glass formed in a submarine environment was found at five KNOX06 dredge sites and in glass-bearing volcanic-rich sediments overlying basaltic basement at DSDP Drill Site 216. Whereas the geochemical characteristics of basaltic whole rocks recovered by drilling and dredging are compromised by seawater–rock alteration processes, the geochemical characteristics of unaltered basaltic glasses are much closer to magmatic compositions. Also, volcanic glass represents melt composition, whereas inferring melt compositions from whole rock compositions can be complicated by the accumulation of phenocrysts. This study focuses on geochemical analyses of the basaltic glasses in order to constrain the petrogenesis of magmas forming the NER.

3. Sample locations and analytical procedures

3.1. Glass-bearing dredges

The dredged KNOX06 glasses occur in rims of pillow basalt fragments and as clasts in palagonite-bearing breccias (Supplementary Fig. 1). They were recovered in five relatively deep dredges (>4 km water depth) distributed along the NER from ~1°N to 19°S (Fig. 1b). The northernmost dredge with glass-bearing samples is Dredge 4 from the steep southeast flank of the seamount drilled and cored at ODP Drill Site 216. Dredge 15 is from the western flank of the NER, at ~8°S. Dredges 25, 26 and 27 are from the steep eastern flank of the NER east and south of ODP Drill Site 757 (for exact location and description of samples see Appendix A in Supplementary Material).

3.2. Glass from drill core sediments at DSDP Drill Site 216

We also analyzed glasses separated from the volcanic, glass-bearing (25 to 40%), clay-rich sediments overlying basement basaltic

flows at DSDP Site 216 (Appendix A). These glasses are from Core 29 section 2 (29-2) and Core 30 sections 2 and 5 (30-2 and 30-5), and are more fully described in Fig. 2 of Keller (2005).

3.3. Analytical procedures

Glass fragments from the dredged samples were chiseled from pillow rims and breccia clasts (Supplementary Fig. 1) or cut into 1–2 mm thick glass slabs with a microwafer saw. These fragments were examined under plane- and cross-polarized light, and isotropic fragments were selected for geochemical analyses. Glass shards from the Site 216 sediments were separated by G. Keller, and isotropic fragments were chosen for this study. Polished glass chips mounted in optical resin, 2–5 chips per sample, were analyzed for major and minor elements by electron microprobe at MIT (Supplementary Table 1) and for trace elements by LA-ICP-MS at Florida State University in 2008, and at Harvard University in 2010 (Supplementary Table 2). Details of analytical procedures are in Appendix B in the Supplementary Material.

4. Results

4.1. Major element composition of NER glasses

Because of low-temperature mobility of alkali metals in a submarine environment, the total alkalis (Na_2O+K_2O) vs. SiO_2 (TAS) plot for classifying tholeiitic and alkalic basalt whole-rocks is unreliable; for example, see the NER whole rock analyses in Fig. 2 of Frey and Weis (1995). However, the hand-picked isotropic glasses analyzed here are relatively unaltered, which is reflected by their near 100% totals (Supplementary Table 1). Consequently, a TAS plot for these NER glasses is a reliable classification plot for distinguishing alkalic and tholeiitic basalt (Fig. 2a). Similar to the submarine-erupted basalt from ODP Drill Site 758 (Frey et al., 1991), glasses from sediments in the DSDP Site 216 drill core and from Dredges 4, 15, 25 and 26 are all tholeiitic basalt, whereas Dredge 27 glasses range from transitional to alkalic basalt. Compared to Southeast Indian Ridge (SEIR) glasses, Dredges 4 and 26 glasses range to lower Na_2O+K_2O, and higher SiO_2, up to 53.2% (Fig. 2a). All the NER glasses define a broad inverse trend between TiO_2 and SiO_2; at a given SiO_2 content Dredge 4 and most of the Dredge 26 glasses have TiO_2 content significantly less than SEIR N-MORB (Fig. 2b).

In a plot of SiO_2 vs. MgO (Fig. 3a), the glasses from Dredges 15, 25 and 27 plot between the fields for flood basalt from the Kerguelen Archipelago and SEIR N-MORB, whereas glasses from Drill Site 216 overlap the field defined by SEIR N-MORB. At a given MgO content, glasses from Dredges 4 and 26 range to the highest SiO_2 contents, exceeding those of SEIR N-MORB. Glasses from Dredges 4 and 15, and Site 216 are Fe-rich (12.46–13.88 wt.%), i.e., they are ferrobasalts (Fig. 3b).

4.2. Incompatible trace element composition of NER glasses

The large range in K_2O and P_2O_5 contents, a factor of 23 and 7, respectively, among these NER glasses (Supplementary Table 1) is consistent with their wide range in primitive mantle-normalized incompatible trace element abundance (Fig. 4). The lowest abundances are in Dredges 4 and 26 glasses (Fig. 4a). The highest abundances are in Dredge 27 glasses, which are markedly enriched in highly incompatible elements; they overlap with flood basalts erupted at Mt. Crozier in the Kerguelen Archipelago (Fig. 4c). In detail, the primitive mantle-normalized plots for the NER glasses are not smooth; specifically, abundance ratios involving elements with similar incompatibility, such as Y/Dy, La/Nb, Zr/Hf, Nb/Ta, and Ce/Pb are generally within analytical error for samples within a dredge, but between dredges these ratios vary significantly and are correlated with Tb/Yb (supplementary Fig. 2), a ratio that is sensitive to a petrogenetic role for garnet (e.g., Frey et al., 2000). The extremes in these ratios are defined by Dredges 26 and 27 glasses.

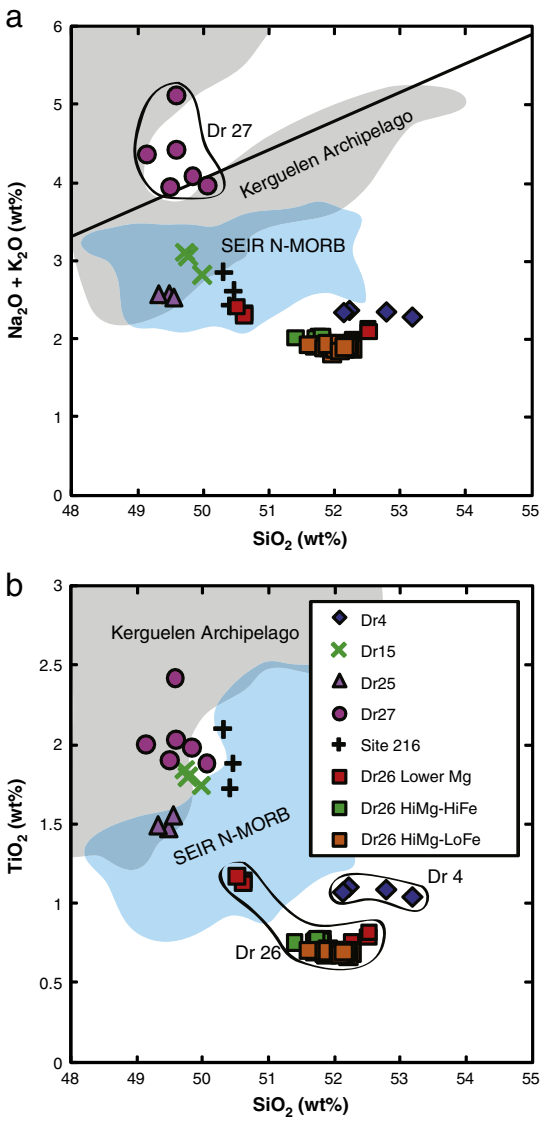

Fig. 2. a. NER glasses in the total alkalis (Na_2O+K_2O) vs. SiO_2 plot used for distinguishing tholeiitic and alkalic basalt. Black dividing line from Macdonald and Katsura (1964). Field for Kerguelen Archipelago flood basalt straddles this boundary line (data from Doucet et al., 2002; Frey et al., 2002; Xu et al., 2007; Yang et al., 1998). SEIR N-MORB are tholeiitic basalts erupted along the SEIR from 78.6° to 113.7°E. Data from Christie et al. (2004) and Douglas-Priebe (1998). Except for Dredge 27 glass, the NER glasses are tholeiitic basalt with the composition of Dredges 4 and 26 glasses extending to higher SiO_2 and lower total alkalis than SEIR N-MORB. In this and subsequent plots Dredge 26 lavas are divided into the three groups (Supplementary Table 1). b. NER glasses in a TiO_2 vs. SiO_2 plot. The source or process that resulted in high SiO_2 also created low TiO_2 contents in Dredge 4 and 26.

Nb/Y vs. Zr/Y (Fig. 5a) was used by Fitton et al. (1997, 2003) to distinguish North Atlantic MORB from the wide range of incompatible element-enriched to -depleted basalt erupted in Iceland. Incompatible element-enriched Icelandic basalts, i.e., high Nb/Y and Zr/Y, and high Nb/Y at a given Zr/Y, are inferred to be derived from the Icelandic hotspot. Incompatible element-depleted Icelandic basalts are also inferred to be derived from the Icelandic hotspot because they are also offset from North Atlantic MORB to higher Nb/Y at a given Zr/Y. This plot is also useful for the NER because, as in Iceland, the NER glasses show a wide range of incompatible element-enriched to -depleted basalt. The incompatible element-enriched NER glasses (i.e., Dredge 27 glasses with high Nb/Y and Zr/Y) overlap with the flood basalts forming the Kerguelen Archipelago that are inferred to have been

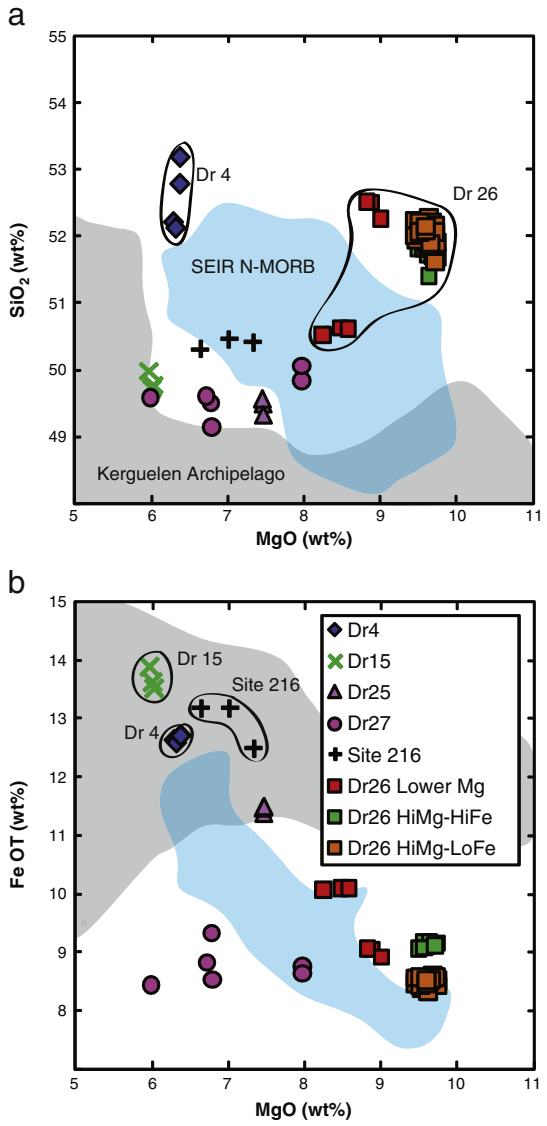

Fig. 3. NER glasses in SiO_2 and FeO (total iron) vs. MgO plots. References for Kerguelen Archipelago and SEIR N-MORB fields in this and all subsequent figures are as in Fig. 3 caption. NER glasses that lie outside these fields are labeled; e.g., the high SiO_2 of Dredge 4 and Dredge 26 glasses. Note that many Dredge 26 glasses have >9% MgO, these "HiMg" glasses have been subdivided based on iron content into "HiFe" (>9% FeO, green squares) and "LoFe" (<8.6% FeO, orange squares) groups. Glasses from Dredges 4 and 15 as well as Drill Site 216 are ferrobasalts (FeO >12.5%).

derived from the Kerguelen hotspot (e.g. Doucet et al., 2005; Weis et al., 1993). Previously studied NER basalts with relatively low incompatible element contents, such as those recovered at Site 758, have been shown to have a significant MORB source component (Weis and Frey, 1991). However, the incompatible element-depleted NER glasses from Dredges 4 and 26 are distinct from the SEIR MORB field; i.e. they have high Nb/Y at a given Zr/Y (Fig. 5a). Consequently, a depleted component that differs from the source of MORB is required to explain incompatible element-depleted basalt erupted in both Iceland and along the NER. As Fitton et al. (1997, 2003) concluded for incompatible element-depleted Icelandic basalt, we suggest that the source of these distinct incompatible element-depleted NER glasses is an intrinsic component of the hotspot.

Fig. 5b uses abundances of the same elements but involves ratios normalized to Nb. Again Dredge 27 glasses overlap with enriched basalt forming the flood basalt of the Kerguelen Archipelago. Basaltic whole-rocks from Drill Sites 756, 757 and 758 as well as basaltic glasses from Drill Site 216 and Dredges 15 and 25 define a trend between the fields for Dredge 27 glasses and SEIR N-MORB. In contrast, the incompatible element-depleted Dredges 4 and 26 lavas define a trend clearly offset to higher Y/Nb at a given Zr/Nb. A similar offset is found in Dredges 4 and 26 whole rocks (Frey et al., 2008). In detail, Dredge 26 glasses range in Zr/Nb from 7.7 to 16.6, and over this range all samples are offset from the trend of MORB to high Y/Nb at a given Zr/Nb. Also, note that the E-MORB and Icelandic fields overlap in Fig. 5a, whereas the SEIR E-MORB field is an extension of the SEIR N-MORB field in Fig. 5b, distinct from the "Depleted-not-MORB" field. Thus, we suggest that Y/Nb vs. Zr/Nb (Fig. 5b) distinguishes two distinct incompatible element-depleted fields, one defined by magmas derived from the MORB source, and the other defined by magmas derived from the hotspot.

4.3. Geochemical characteristics of glasses in volcanic-rich sediments at Site 216

The ferrobasalts, FeO/MgO >2 and FeO >13.8% (e.g. Ludden et al., 1980), forming the uppermost basement at Drill Site 216 are relatively enriched in incompatible elements (Fig. 4d). Also they have relatively high $^{87}Sr/^{86}Sr$ (0.7054) and low $^{143}Nd/^{144}Nd$ (ε_{Nd}~0.6) ratios that overlap with the field proposed for the Kerguelen hotspot (Frey and Weis, 1995).

The glasses in volcanic-rich sediment overlying Drill Site 216 igneous basement are also ferrobasalt with FeO/MgO >1.7 and FeO >12.5% (Fig. 3b). These glasses are moderately enriched in incompatible element content and glass sample 30-2 is most similar to the underlying ferrobasalt flows (Fig. 4d). All ferrobasalts at Site 216, i.e. both whole-rocks and glasses are relatively depleted in Sr and Eu, i.e, $(Sr/Nd)_{PM} = 0.58–0.72$ and $Eu/Eu^* = 0.53–0.70$ where the PM subscript indicates normalization to Hofmann, 1988 values, and * indicates the expected value assuming linearity between the two adjacent elements on the PM normalized incompatible element plot. Because Sr is compatible in plagioclase (e.g., Bedard, 2006), this result is consistent with the major role for fractionation of plagioclase required to generate ferrobasalt (e.g., Ludden et al., 1980).

The glass-rich volcanic clay overlying basement basalt at Drill Site 216 may be eroded material from the basaltic basement, or reflect late-stage volcanism from the Drill Site 216 seamount or eruption products from a younger NER volcano. The presence of unaltered glass and its compositional similarity to Drill Site 216 basement ferrobasalt is consistent with a local source for the glass-bearing volcanic clays. In addition, the presence of basaltic glasses with evolved compositions, such as ferrobasalt in Dredges 4 and 15 and Drill Site 216 (Fig. 3b), in the uppermost NER igneous basement likely reflects a decrease in magma eruption rate thereby enabling sufficient time for extensive crystal fractionation as observed at Hawaiian volcanoes when they move away from the hotspot (e.g., Frey et al., 1990).

5. Discussion

We focus our petrogenetic inferences on Dredge 4 and 26 glasses because:

a) They have low abundances of incompatible trace elements, within the range defined by SEIR N-MORB (Fig. 4a), but they differ from MORB in ratios involving Nb, Zr and Y (Fig. 5).
b) They are distinctly different from SEIR N-MORB in major element composition; specifically they have higher SiO_2 and FeO at a given MgO content (Fig. 3).
c) Dredge 26 glasses have relatively high MgO contents, 8.2 to 9.7%, (Fig. 3), and are aphryic to sparsely olivine-phyric. Consequently, they have experienced less post-melting processing than glasses from other dredges.

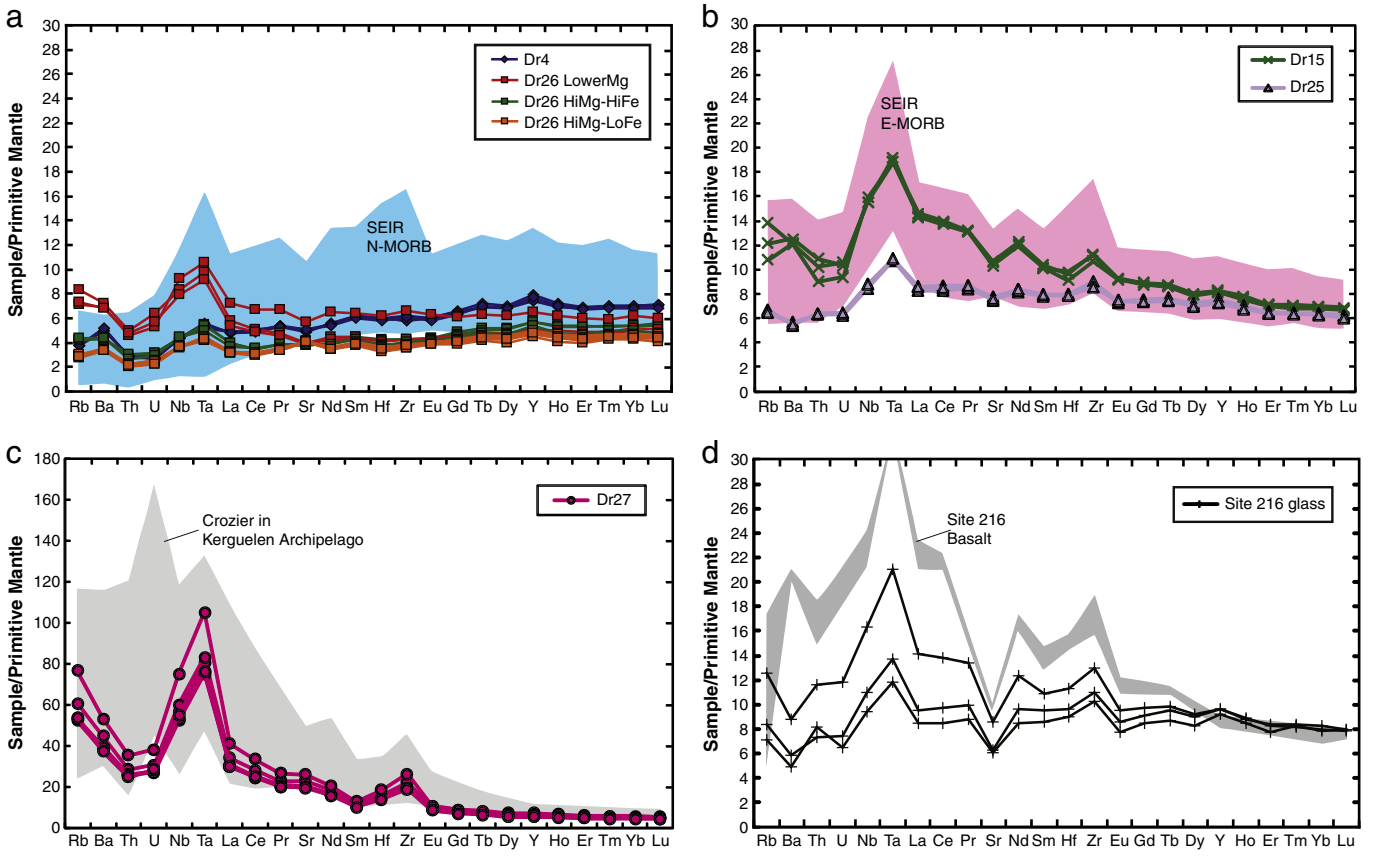

Fig. 4. Primitive mantle (Hofmann, 1988) normalized plot for incompatible elements in NER glasses. Notable is the diversity of patterns: Dredge 4 glasses are like N-MORB and Dredge 26 glasses are PM-like, except for the lower-Mg Dredge 26 samples that are relatively enriched in Nb and Ta. Dredge 27 alkalic basalt glasses are strongly enriched in the most incompatible elements (note vertical scale is 0 to 180) and are similar to the alkalic flood basalt exposed in the Mt. Crozier section of flood basalt in the Kerguelen Archipelago. Dredges 15 and 25 are like E-MORB. Site 216 glasses and whole-rocks (Frey and Weis, 1995) are also relatively enriched in highly incompatible elements, although Sr and Eu are depleted relative to their adjacent elements.

5.1. Petrogenesis of Dredges 4 and 26 glasses

5.1.1. Constraints from Dredge 26 major element composition

Glasses with relatively high MgO contents (greater than 9.4%), like those recovered at Dredge 26, are rare in the ocean basins. Two well-documented areas where such glasses occur are the Siqueiros Fracture Zone on the East Pacific Rise (e.g., Herzberg et al, 2007; Perfit et al., 1996), and along the Galapagos Spreading Center north of the Galapagos Archipelago (e.g., Christie and Sinton, 1981; 1986). The highest MgO glasses from the Siqueiros Fracture Zone were recovered along a short transform fault between two intra-fracture zone spreading segments. The highest MgO glasses from the Galapagos Spreading Center were dredged from the bathymetric low at the tip of the propagating rift at 95.5°W. The occurrence of high MgO glasses at these locations is attributed to magma eruption with little or no residence time in the lithosphere, thereby inhibiting both prolonged fractional crystallization and mixing in axial magma chambers (e.g., Christie and Sinton, 1981; Gregg et al., 2009). We suggest that the Dredge 26 glasses recovered from the base of a deep, north–south striking scarp (Fig. 1b) erupted in an analogous tectonic environment.

Relative to the compositional field of SEIR MORB, most of the Dredge 26 glasses have significantly higher SiO_2 and FeO contents (Fig. 3b). The occurrence of both relatively high SiO_2 and FeO is counter to the common generalization that high SiO_2 content reflects melt segregation at low pressure whereas high FeO content reflects melt segregation at high pressure (e.g., Jacques and Green, 1980; Klein and Langmuir, 1987). What are the implications of the relatively high SiO_2 and FeO in Dredge 26 glasses?

If the high MgO magmas from these three locations have experienced only olivine fractionation, we can calculate the initial and final pressures of melting, the extent of melting, and the olivine fractionation path of an accumulated fractional melt by using the approach of Herzberg and O'Hara (2002). For the relatively aphyric to sparsely olivine–phyric NER Dredge 26 glasses, olivine-only fractionation is probably valid only for glasses with MgO >9.5%; we divide these high MgO Dredge 26 glasses into high FeO (~9.1%, n = 8) and low FeO (~8.5%, n = 30) groups (Fig. 3b, Supplementary Table 1). An examination of the entire Siqueiros Fracture Zone suite (Perfit et al., 1996) suggests that olivine-only fractionation is probably valid for glasses with MgO>~9.8%. We use the lowest MgO glass from this most primitive Siqueiros group as the closest comparison to the Dredge 26 lavas (AII1991-020-015, 9.89% MgO). For Galapagos Spreading center glasses Cushman et al. (2004) suggested that plagioclase and/or clinopyroxene began to crystallize at about 8.5% MgO; however, Christie and Sinton (1986) preferred to model parental magmas using the most primitive set of glasses, 9.42% MgO (the average of 60 samples dredged from a site at the tip of the 95.5 W propagator). This MgO content is similar to the NER Dredge 26 and Siqueiros glasses, so we use that composition for modeling the Galapagos melting path. The major element composition of each modeled glass is in Supplementary Table 3.

We calculate primary melt compositions for each glass using the PRIMELT2 implementation of the Herzberg and O'Hara (2002) model after Herzberg and Asimow (2008). The approach involves two types of calculations: (1) a backward fractionation model that generates a series of melt compositions by adding incremental amounts of

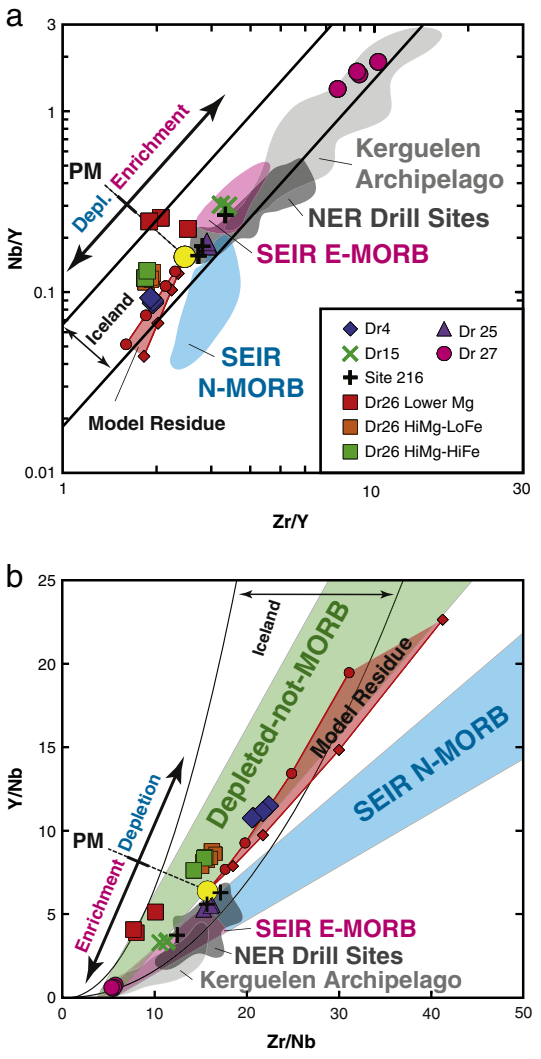

Fig. 5. a. A Nb/Y vs. Zr/Y plot was used by Fitton et al. (1997, 2003) to distinguish North Atlantic N-MORB from the wide range of incompatible element-enriched to -depleted hotspot-derived basalts erupted in Iceland. Black lines indicate the Iceland array from Fitton et al. (1997) and, as with North Atlantic N-MORB, this field largely separates NER glasses from SEIR N-MORB. Modeling calculations of Fitton et al., 1997 show that the trends of melts and residues formed by varying extents of melting of a common source are parallel to the Icelandic field defined by the black lines. Also fields are shown for Kerguelen flood basalt (light gray) and NER Drill Sites 216, 756, 757, and 758 (dark gray; Frey and Weis, 1995; Frey et al., 1991). As in Iceland, NER samples range from incompatible element-enriched to -depleted basalt, but the incompatible element depleted NER basalt is distinct from SEIR MORB (i.e. Dredge 4 and Dredge 26 glasses have higher Nb/Y at a given Zr/Y than SEIR N-MORB). Consequently, a depleted component that differs from MORB is required to explain both Icelandic and NER basalt; apparently it is a depleted hotspot component. PM is the primitive mantle estimate of Hofmann (1988). b. This plot uses abundances of the same elements as Fig 5a, but involves ratios normalized to Nb. Again Dredge 27 glasses overlap with enriched basalt forming the flood basalt of the Kerguelen Archipelago, whereas the depleted Dredges 4 and 26 lavas clearly define a trend offset from the MORB field to higher Y/Nb at a given Zr/Nb. This offset to high Y/Nb can be explained if Dredges 4 and 26 glasses were derived from a garnet-bearing peridotite created as a residue in a prior melting event. The Y anomalies, i.e., Y peaks in primitive mantle-normalized plots (Fig. 4) and high Y/Nb at a given Zr/Nb, in Dredges 4 and 26 glasses are confirmed by X-ray fluorescence data for Dredge 4 and 26 whole-rocks (Frey et al., 2008). In both panels the red diamonds and circles define model residue fields created by 0.5–3% fractional melting of a Primitive Mantle source (Hofmann, 1988); see Appendix C for details of calculation.

equilibrium olivine to the chosen glass composition; for each melt composition along the olivine addition trend a melt fraction is determined from the MgO and FeO content of the melt (see equations 1 and 3 of Herzberg and Asimow, 2008), and (2) a forward model that calculates a series of accumulated fractional melts based on a parameterization of experimental data for partial melting of a fertile peridotite (Walter, 1998). These two types of calculations yield a unique primary melt composition for each chosen glass composition when there is a common melt fraction for the accumulated fractional melts created by partial melting of the fertile peridotite and the melts created by olivine addition (Herzberg and Asimow, 2008).

Fig. 6 is a graphical presentation of the modeling results for each glass in Supplementary Table 3. The initial melt composition, specifically MgO, FeO, and SiO_2 contents, varies with pressure along the mantle solidus, as shown by the red line in Fig. 6. Also, several possible decompression melting paths are shown in green, and the final pressure of melting is contoured in blue. The melting paths of the two high MgO Dredge 26 groups are shown in magenta, the Galapagos Spreading Center glass melting path is in orange, and the Siqueiros Fracture Zone glass melting path is in blue. The measured glass compositions are shown by large colored circles, and olivine addition paths, in one percent increments, are the small yellow circles. An important observation is that the primary magma compositions for the Dredge 26 and Galapagos glasses began melting along the garnet peridotite solidus, but the primary melt for the Siqueiros glass began melting along the spinel peridotite solidus, that is, at significantly lower pressure. Note that the initial pressure of melting correlates positively with FeO content; e.g., the high FeO group of Dredge 26 glasses reflect the highest pressure of initial melting. On the other hand, relatively high SiO_2 contents, characteristic of Dredge 26 glasses (Fig. 3a), are usually explained by melt segregation at relatively low pressures (e.g., Klein and Langmuir, 1987). This is also true for the Dredge 26 glasses, note that melting continued to less than 1 GPa (Fig. 6). In summary, the NER Dredge 26 glasses have relatively high FeO contents because melting commenced at relatively high pressure, and they have relatively high SiO_2 contents because melting continued to relatively low pressures (Fig. 6).

The relative lengths of the melting columns in Fig. 6 show that the degree of melting was greater for Dredge 26 glasses than for the other examples, nearly 30% for the Dredge 26 glasses, about 25% for the Galapagos glasses, and less than 10% for the Siqueiros Fracture Zone glass. Such a high extent of melting for Dredge 26 glasses is consistent with their relatively low TiO_2 and incompatible trace element abundance (Figs. 2b and 4a). At 30% extent of melting, both garnet and clinopyroxene are exhausted in the mantle source, leaving a harzburgite residue, and creating a melt with incompatible trace element abundance ratios closely reflecting those of the mantle source.

5.1.2. Petrogenetic inferences based on a Y anomaly

In Fig. 5b, we showed that Dredge 4 and 26 glasses are offset from most OIB and MORB to high Y/Nb at a given Zr/Nb. Although this offset could reflect either anomalously low Zr or high Y abundance, we note that in a primitive mantle-normalized plot Dredge 4 and 26 glasses exhibit positive Y anomalies (Fig. 4a), as shown by their relatively high Y/Dy ratios (Supplementary Fig. 2). Dredges 4 and 26 glasses share the distinctive feature of high SiO_2 content relative to MORB, but Dredge 4 glasses have much lower MgO and higher FeO contents (Fig. 3). We infer that Dredge 4 and 26 glasses were derived from similar parental magma compositions, but the evolved nature of Dredge 4 glasses reflects post-melting fractionation of clinopyroxene and plagioclase in addition to olivine. This is consistent with their Sr and Eu anomalies, $(Sr/Nd)_{PM} = 0.87–0.95$ and $Eu/Eu^* = 0.93–0.99$), indicative of plagioclase fractionation, but we emphasize that fractional crystallization of these phases will not significantly change Y/Dy ratios.

The ionic radius of the Y^{+3} cation is very similar to that of the rare earth elements Dy and Ho (Pack et al., 2007; Whitaker and Muntus, 1970). Consequently, in primitive mantle and chondrite normalized plots, Y is commonly plotted between Ho and Dy (e.g., McDonough and Sun, 1995). This location reflects the similarity of partition coefficients for Dy, Y and Ho during partial melting of mantle peridotite. However, some minerals, notably garnet, can significantly fractionate Y from Ho and Dy (Van Westrenen and Draper, 2007). Specifically, D_Y/D_{Ho} and

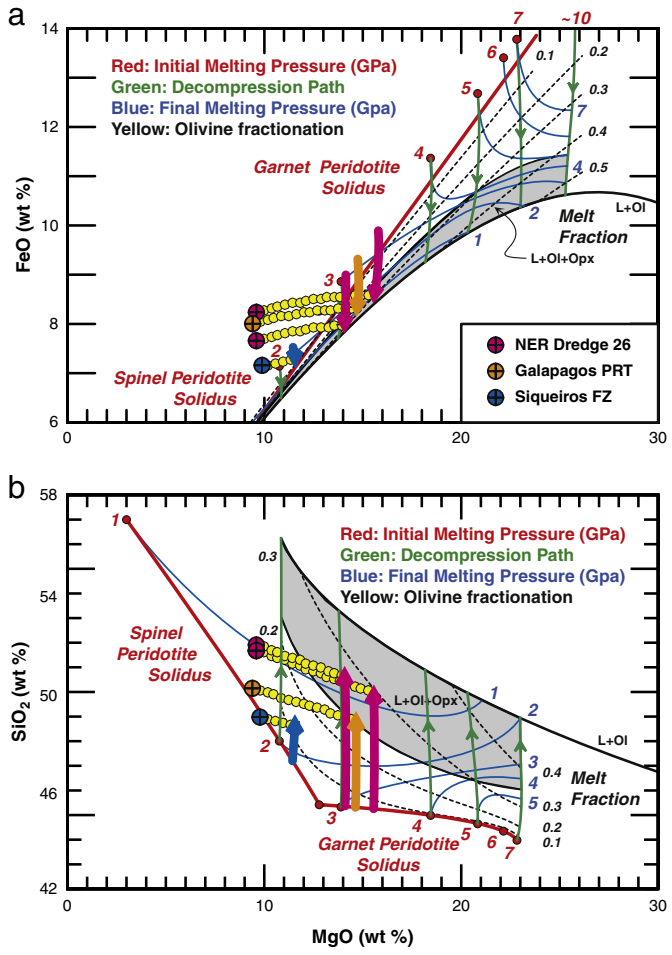

Fig. 6. Hybrid forward melting and crystallization model for average Dredge 26 high Mg, high Fe and low Fe glass compositions, compared to a primitive glass from the Siqueiros Fracture Zone (Perfit et al, 1996), and the average glass dredged from the propagating rift tip of the Galapagos Spreading Center at 95.5° W (Christie and Sinton, 1981, 1986). The original hybrid model was described in Herzberg and O'Hara (2002); here we use the PRIMELT2 graphical projections after Herzberg (2006) and Herzberg et al. (2007). Initial melting occurs along the solidus (red line), several possible decompression melting paths are shown in green, and final pressure of melting is contoured in blue. The melting paths of the two Dredge 26 groups are shown in magenta, the Galapagos Spreading Center glass melting path is shown in orange, and the Siqueiros Fracture Zone glass melting path is shown in blue. Small yellow circles show subsequent olivine-only crystallization paths in one weight percent increments, and end in the erupted glass compositions shown with large colored circles. Note that melting for the NER and Galapagos glasses began along the garnet peridotite solidus, but that the Siqueiros glass began melting at a significantly lower pressure along the spinel peridotite solidus. Also, FeO content of the glasses correlates positively with initial melting pressure, i.e., the Dredge 26 high FeO group began melting at the highest pressure. The relatively high SiO_2 content of the Dredge 26 glasses is due to melting continuing to low pressures, less than 1 GPa. The significantly greater length of the Dredge 26 melting columns also leads to a significantly higher extent of melting (contoured in dashed black lines), nearly 30% for the Dredge 26 glasses, in contrast to 25% for the Galapagos propagating rift tip glass, and significantly less than 10% for the Siqueiros Fracture Zone glass.

D_Y/D_{Dy} garnet/melt partition coefficients range from 1.2 to 1.5 and 1.2 to 2.1, respectively (Pertermann et al., 2004; Tuff and Gibson, 2007). Residual garnet during a partial melting process is also very effective in creating relatively low Y/Nb in partial melts and complementary high Y/Nb in a garnet-bearing residue (Fig. 5b). Consequently, we attribute the high Y/Nb as well as the high Y/Dy and low Tb/Yb in Dredge 4 and 26 glasses (Fig. 4a, 7b, and Supplementary Fig. 2) as resulting from high extents of melting of a garnet-bearing peridotite created as a residue in a partial melting event.

The relatively low abundances of TiO_2 and incompatible trace elements in Dredge 4 and 26 glasses (Figs. 2b and 4a) are consistent with these glasses being derived from a depleted source, such as a residual peridotite created during an earlier partial melting event. If this residue was garnet- and clinopyroxene-bearing, it would have high Y/Nb and Y/Dy and low Tb/Yb. Moreover, if this residual garnet lherzolite was melted to 30% (Fig. 6), the residue would contain only olivine and orthopyroxene. Because these two minerals have very low, <<1, solid/melt partition coefficients for Y, Nb, Zr and REE (e.g., Fitton et al., 1997), partial melts formed at such high extents of melting inherit the incompatible element ratios of their sources, e.g., the high Y/Nb and Y/Dy and low Tb/Yb of residual garnet-lherzolite (Fig. 4a, 7b, and Supplementary Fig. 2).

5.1.3. Source composition constraints from combined Nb–Y–Zr relationships

The differences between the Depleted-not-MORB and SEIR N-MORB fields in Fig. 5 could reflect Nb-enrichment and/or Zr depletion in the Depleted-not-MORB NER lavas (Fig. 5a) and Y-enrichment and/or Zr-depletion (Fig. 5b). Note that a Zr deficit, if present, would be apparent in both Fig. 5a and b, whereas Nb/Y vs. Zr/Y is insensitive to Y enrichment or depletion, and Y/Nb vs. Zr/Nb is insensitive to Nb enrichment or depletion.

In Fig. 7, we test for Nb, Y and Zr anomalies separately, using PM-normalized ratios of Nb/La, Y/Dy, Nb/Y, and Zr/Sm vs. La/Sm. Fig. 7a shows that Dredge 26 glasses are offset from the SEIR MORB field to high Nb/La at a given La/Sm, whereas Dredges 4 and 26 glasses are offset to higher Y/Dy than SEIR MORB (Fig. 7b). Fig. 7c shows that both Dredges 4 and 26 glasses are offset to lower Zr/Sm than SEIR MORB. In contrast, Fig. 7d shows that Dredge 4 and high MgO Dredge 26 glasses overlap the SEIR MORB field; apparently the Nb and Y enrichments are of similar magnitude and cancel each other out. Fig. 7a and b also show that the calculated trends for garnet-bearing residues cannot explain the Nb/La and Y/Dy differences between the sources of SEIR MORB and Dredge 26 glasses. Consequently we infer that these differences in Nb, Y, and Zr are related to differences in source composition, i.e., relative to the source of SEIR MORB, the source of Dredge 26 glasses was enriched in Nb and Y and depleted in Zr.

Fitton et al. (1997) used a plot of Nb/Y vs. Zr/Y (Fig. 5a) to conclude that both incompatible element-enriched and -depleted Icelandic basalts are relatively enriched in Nb. They inferred that all Icelandic basalts are derived from Nb-enriched residues created during partial melting in an arc environment; subsequently these residues were recycled into the mantle, and provided a source of depleted Icelandic basalt.

We suggest that a significant amount of the offset seen in Y/Nb vs. Zr/Nb (Fig. 5b) could result from melting a garnet-bearing peridotite residue with Y enrichment due to residual garnet. Similarly, a deficiency in Zr, as manifested by low Zr/Sm in the melt (Fig. 7c), is a signature of residual clinopyroxene (Chauvel and Hemond, 2000). Although the clinopyroxene partition coefficient ratio for Zr/Sm is less than one, this ratio for garnet/melt is greater than one. Consequently, the Zr/Sm ratio is sensitive to the relative proportion of garnet and clinopyroxene in the residue.

In summary, the major and trace element abundances of Dredges 4 and 26 glasses show that they were derived by high extents (~30%) of melting of garnet lherzolite residues created during a previous partial melting event, perhaps by magmatic processes occurring in arc environments and this depleted source is not the source of SEIR MORB.

5.2. Diversity of mantle sources contributing to volcanism on the Ninetyeast Ridge

Based on the geochemical characteristics of NER basaltic basement recovered at ODP Drill Sites 756, 757 and 758, and DSDP Site 216, Frey and Weis (1995) and Weis and Frey (1991) concluded that NER magmas were generated by mixing between at least three source

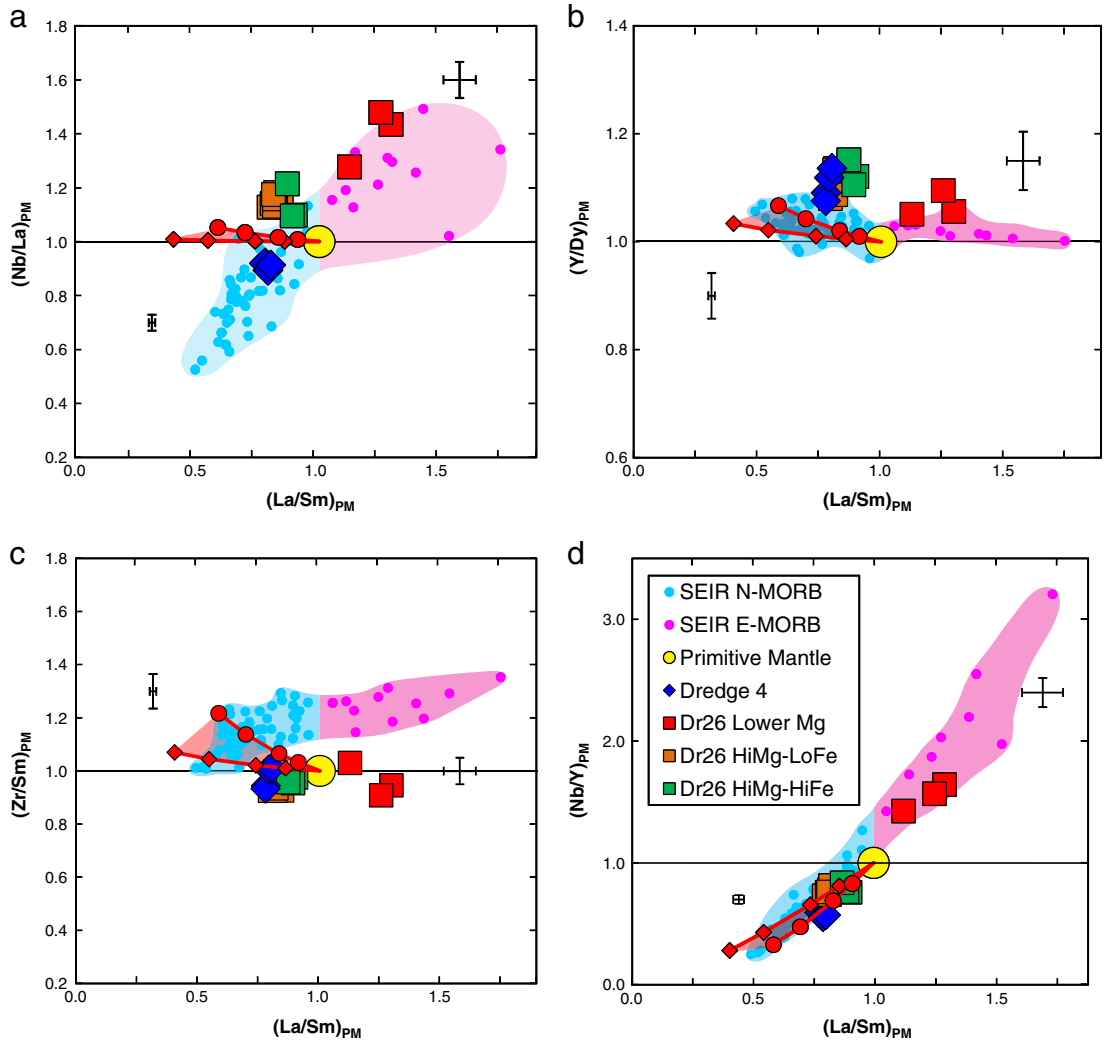

Fig. 7. $(Nb/La)_{PM}$, $(Y/Dy)_{PM}$, $(Zr/Sm)_{PM}$ and $(Nb/Y)_{PM}$ vs. $(La/Sm)_{PM}$. Subscript PM indicates normalized to primitive mantle (indicated by large yellow circle) (Hofmann, 1988). These ratios involve elements of very similar incompatibility; however, specific minerals can change these ratios, e.g., rutile for Nb/La and garnet for Y/Dy. $(La/Sm)_{PM} = 1$ distinguishes SEIR E- and N-MORB. Red circles and diamonds represent the range of modeled melt residues (see Appendix C for details). a and b: the high Mg, low and high FeO Dredge 26 glasses are offset from SEIR N-MORB to high Nb/La and Y/Dy at a given La/Sm. Similarly, the low MgO Dredge 26 glasses have higher ratios than SEIR E-MORB. Dredge 4 glasses are offset to high Y/Dy but not to high Nb/La. c: All Dredges 4 and 26 glasses are offset from SEIR N- and E-MORB to low Zr/Sm at a given La/Sm. d: Dredges 4 and 26 glasses are not significantly offset from SEIR MORB; the Nb and Y offsets in panels a and b cancel each other, i.e., Nb and Y were equally enriched in the source of Dredges 4 and 26 glasses. Although not shown, Icelandic basalts are also offset from North Atlantic MORB to high Nb/La, high Y/Dy and low Zr/Sm.

components: a depleted MORB-component and two different enriched ocean island basalt (OIB) components. Radiogenic isotope analyses (i.e., Sr, Nd, Pb, and Hf isotopic ratios), are necessary to differentiate the two enriched OIB components (Nobre Silva et al., 2007). However, both the alkalic basalt glasses from Dredge 27 and alkalic flood basalts erupted in the Kerguelen Archipelago are highly enriched in the most incompatible elements (e.g., $(La/Yb)_{PM}$ is 6.0 to 8.7 in Dredge 27 glasses, Fig. 4c). Relative to primitive mantle, Dredge 27 glasses have high Zr/Hf (~50) and Ce/Pb (~30) and low La/Nb (~0.5) and Nb/Ta (~14) (Supplementary Fig. 2). These geochemical characteristics are consistent with derivation of Dredge 27 lavas from a garnet and clinopyroxene-bearing source having the geochemical signature of recycled oceanic crust; specifically, their high La/Yb and Zr/Hf reflecting residual garnet and clinopyroxene respectively, high Ce/Pb reflecting fluid loss in a sub-arc environment and low La/Nb and Nb/Ta reflecting residual rutile in the recycled oceanic crust (Klemme et al., 2005).

In addition to the Kerguelen-like component, we have found evidence for a depleted source with geochemical characteristics that are distinct from the source of SEIR MORB. Specifically, Dredge 4 and high MgO Dredge 26 glasses are MORB-like in that they are relatively depleted in the most highly incompatible elements (Fig. 4a). Despite this similarity, abundance ratios among the high field strength elements Y, Zr and Nb show that the depleted component expressed in Dredge 4 and 26 glasses is distinct from SEIR MORB (Fig. 5b); hence depleted sources related to the hotspot are inferred. This scenario is identical to that proposed by Fitton et al. (1997) for the origin of incompatible element-depleted Icelandic basalts from a source intrinsic to the Icelandic hotspot. However, a hotspot-related depleted source has not been previously identified as a source component for NER lavas.

Finally, although in some figures (e.g., Supplementary Fig. 2) some NER basalts define trends consistent with a MORB mixing component, drilling and dredging along the NER has not recovered any basalt that has all the geochemical characteristics of SEIR MORB.

6. Conclusions

The major and trace element compositions of basaltic glass from six locations along the Ninetyeast Ridge (NER) are diverse. They range from incompatible element-rich alkalic basalt (Dredge 27) to

tholeiitic ferrobasalt (Dredge 15 and Drill Site 216) to incompatible element-depleted tholeiitic basalts (Dredges 4 and 26). These results lead to several conclusions:

(1) The Dredge 27 alkalic basalt compositions provide evidence for a Kerguelen hotspot-like source contributing to NER magmatism.
(2) The common occurrence of ferrobasalt in uppermost NER igneous basement (Dredges 4 and 15, DSDP Site 216) is consistent with a decreasing supply of basaltic magma from the mantle thereby providing sufficient time for plagioclase-dominated fractional crystallization within the crust. As at Hawaiian volcanoes, the decreasing magma supply is inferred to be characteristic of hotspot volcanism as a volcano migrates away from the hotspot.
(3) The major element compositions of high MgO (>9.5%) glasses from Dredge 26 are consistent with nearly 30% partial melting of a garnet-bearing peridotite over a large pressure interval, from slightly over 3 to less than 1 GPa.
(4) The inferred trace element characteristics of the peridotite source of Dredges 4 and 26 glasses, that is, low abundances of incompatible elements and abundance ratios of high-field-strength elements that differ from those of MORB, indicate that it formed as a garnet- and clinopyroxene-bearing residual peridotite created during a partial melting event. Subsequently this residual peridotite with the trace element characteristics of garnet and clinopyroxene was melted to approximately 30%, thereby generating the parental melts of Dredge 4 and 26 glasses.
(5) At least 4 mantle source components are necessary to generate the basaltic compositions found along the NER. Three of these components can be distinguished using incompatible trace element compositions alone: two relatively depleted sources, and a relatively enriched source. Radiogenic isotope analyses (i.e., Sr, Nd, Hf, and Pb) are needed to differentiate the distinct enriched sources that have been identified in other studies.

Supplementary materials related to this article can be found online at doi:10.1016/j.epsl.2010.12.051.

Acknowledgements

We thank Chief Scientist W. Sager and the officers and crew of the RV Revelle for their shipboard expertise, R. Comer for supervising the dredging operation, and the students who sorted and described the dredged rocks (S. Baumgartner, E. Gauntlett, S. Mallick, E. Mervine, I. Nobre Silva, H. Owens, S. Rasmussen, and J. Wiltshire).

We thank G. Keller for providing glasses picked from sediments overlying basaltic basement at Drill Site 216. D. Graham provided a digital version of the electron microprobe compostions reported by Douglas-Priebe (1998) and D. Pyle provided an enhanced version of the Christie et al, 2004 PetDB data submission.

Profs. M. Humayun, V. J. M. Salters, and C. H. Langmuir are thanked for access to their LA-ICP-MS facilities at FSU and Harvard. LA-ICP-MS technical support from T. Zateslo and Z. Chen is also highly appreciated. Last but not least, C. Herzberg is thanked for numerous and stimulating discussions regarding magma compositions derived from peridotite and pyroxenite.

Finally, we thank reviewers A. le Roex and G. Fitton and Editor R. Carlson for their comments on the submitted manuscript.

This research was supported by NSF grant OCE-0825147.

References

Bedard, J.H., 2006. Trace element partitioning in plagioclase. Geochim. Cosmochim. Acta 70, 3717–3742.
Chauvel, C., Hemond, C., 2000. Melting of a complete section of recycled oceanic crust; trace element and Pb isotopic evidence from Iceland. Geochem. Geophys. Geosyst. 1 (2), 1001. doi:10.1029/1999GC000002.
Christie, D.M., Sinton, J.M., 1981. Evolution of abyssal lavas along propagating segments of the Galapagos spreading center. Earth Planet. Sci. Lett. 56, 321–335.
Christie, D.M., Sinton, J.M., 1986. Major element constraints on melting, differentiation and mixing of magmas from the Galapagos 95.5 degrees W propagating rift system. Contr. Mineral. Petrol. 94, 274–288.
Christie, D.M., Pyle, D.G., Sylvander, B.A., 2004. Submitted Data Set: Major and Trace Element Composition of Basalts from the Southeast Indian Ridge (Westward Cruise, leg 10). http://www.petdb.org. Accessed July, 2009.
Cushman, B., Sinton, J., Ito, G., Dixon, J.E., 2004. Glass compositions, plume\ridge interaction, and hydrous melting along the Galapagos Spreading Center, 90.5 W to 98 W. Geochem. Geophys. Geosyst. 5. doi:10.1029/2004GC000709. Q08E17,.
Doucet, S., Weis, D., Scoates, J.S., Nicolaysen, K., Frey, F.A., Giret, A., 2002. The depleted mantle component in Kerguelen Archipelago basalts: petrogenesis of tholeiitic-transitional basalts from the Loranchet Peninsula. J. Petrol. 43, 1341–1366.
Doucet, S., Scoates, J.S., Weis, D., Giret, A., 2005. Constraining the components of the Kerguelen mantle plume: a Hf–Pb–Sr–Nd isotopic study of picrites and high-MgO basalts from the Kerguelen Archipelago. Geochem. Geophys. Geosyst. 6, Q04007. doi:10.1029/2004GC000806.
Douglas-Priebe, L.M., 1998. Geochemical and petrogenetic effects of the interaction of the Southeast Indian Ridge and the Amsterdam-St. Paul Hotspot. MS Thesis, Oregon State University, Oregon.
Fitton, J.G., Saunders, A.D., Norry, M.J., Hardarson, B.S., Taylor, R.N., 1997. Thermal and chemical structure of the Iceland plume. Earth Planet. Sci. Lett. 153, 197–208.
Fitton, J.G., Saunders, A.D., Kempton, P.D., Hardson, B.S., 2003. Does depleted mantle form an intrinsic part of the Iceland plume? Geochem. Geophys. Geosyst. 4 (3), 1032. doi:10.1029/2002GC000424.
Frey, F.A., Weis, D., 1995. Geochemical constraints on the origin and evolution of the Ninetyeast Ridge: a 5000 km hotspot trace in the eastern Indian Ocean. Contr. Mineral. Petrol. 121, 18–28.
Frey, F.A., Wise, W.S., Garcia, M.O., West, H., Kwon, S.-T., Kennedy, A., 1990. Evolution of Mauna Kea volcano, Hawaii: petrologic and geochemical constraints on postshield volcanism. Jour. Geophys. Res. 95, 1271–1300.
Frey, F.A., Jones, W.B., Davies, H., Weis, D., 1991. Geochemical and petrologic data for basalts from Site 756, 757, and 758: implications for the origin and evolution of Ninetyeast Ridge. Proc. ODP Sci. Results 121, 611–659.
Frey, F.A., Clague, D., Mahoney, J.J., Sinton, J.M., 2000. Volcanism at the edge of the Hawaiian plume: petrogenesis of submarine alkalic lavas from the North Arch volcanic field. J. Petrol. 41 (5), 667–691.
Frey, F.A., Nicolaysen, K., Kubit, B.K., Weis, D., Giret, A., 2002. Flood basalt from Mont Tourmente in the Central Kerguelen Archipelago: the change from transitional to alkalic basalt at 25 Ma. J. Petrol. 43, 1367–1387.
Frey, F.A., Pringle, M., Piotrowski, A., Gauntlett, E., Huang, S., Mervine, E., 2008. Geochemical constraints on the origin of the Ninetyeast Ridge, Indian Ocean, Eos Trans. AGU Fall Meet. Suppl. Abstr. 89 (53), T58B-04.
Gregg, P.M., Behn, M.D., Lin, J., Grove, T.L., 2009. Melt generation, crystallization, and extraction beneath segmented oceanic transform faults. J. Geophys. Res. 114, B11102. doi:10.1029/2008JB006100.
Herzberg, C., 2006. Petrology and thermal structure of the Hawaiian plume from Mauna Kea volcano. Nature 444, 605–609. doi:10.1038/nature05254.
Herzberg, C., Asimow, P.D., 2008. Petrology of some oceanic island basalts: PRIMELT2. XLS software for primary magma calculation. Geochem. Geophys. Geosyst. 9, Q09001. doi:10.1029/2008GC002057.
Herzberg, C., O'Hara, M.J., 2002. Plume-associated ultramafic magmas of Phanerozoic age. J. Petrol. 43, 1857–1883. doi:10.1093/petrology/43.10.1857.
Herzberg, C., Asimow, P.D., Arndt, N., Niu, Y., Lesher, C.M., Fitton, J.G., Cheadle, M.J., Saunders, A.D., 2007. Temperatures in ambient mantle and plumes: constraints from basalts, picrites, and komatiites. Geochem. Geophys. Geosyst. 8, Q02006. doi:10,1029/2006GC001390.
Hofmann, A.W., 1988. Chemical differentiation of the earth: the relationship between mantle, continental crust and oceanic crust, Earth Planet. Sci. Lett. 90, 297–314.
Jacques, A.L., Green, D.H., 1980. Anhydrous melting of peridotite at 0–15 kb pressure and genesis of tholeiitic basalts. Contrib. Mineral. Petrol. 73, 287–310.
Keller, G., 2005. Biotic effects of late Maastrichtian mantle plume volcanism: implications for impacts and mass extinctions. Lithos 79, 317–341.
Klein, E.M., Langmuir, C.H., 1987. Global correlations of ocean ridge basalt chemistry with axial depth and crustal thickness. J. Geophys. Res. 92, 8089–8115.
Klemme, S., Prowatke, S., Hametner, K., Gunther, D., 2005. Partitioning of trace elements between rutile and silicate melts: implications for subduction zones. Geochim. Cosmochim. Acta 69 (9), 2361–2371.
Ludden, J.N., Thompson, G., Bryan, W.B., Frey, F.A., 1980. The origin of lavas from the Ninetyeast Ridge, Eastern Indian Ocean: an evaluation of fractional crystallization models. Jour. Geophys. Res. 85, 4405–4420.
Macdonald, G.A., Katsura, T., 1964. Chemical composition of Hawaiian lavas. J. Petrol. 5, 82–133.
McDonough, W.F., Sun, S.S., 1995. The composition of the Earth. Chem. Geol. 120, 223–253.
Nobre Silva, I., Weis, D., Scoates, J.S., Frey, F.A., 2008. Ninetyeast Ridge Knox06RR: high-precision isotopic compositions from new dredge samples. Eos Trans. AGU Fall Meet. Suppl. Abstr. 89 (53), T54B-05.
Nobre Silva., I., Weis, D., Swinnard, L., Scoates, J.S., 2007. Ninetyeast Ridge, Indian Ocean: constraining its origin and relation with the Kerguelen, Amsterdam, and St. Paul hotspots. Geochim. Cocmochim. Acta 71 (15) Supplement 3, A721.
Pack, A., Russell, S.S., Michael, J., Shelley, G., Zuilen, M., 2007. Geo- and cosmochemistry of the twin elements yttrium and holmium. Geochim. Cosmochim. Acta 71, 4592–4608.

Perfit, M.R., Fornari, D.J., Ridley, W.I., Kirk, P.D., Casey, J., Kastens, K.A., Reynolds, J.R., Edwards, M., Desonie, D., Shuster, R., Paradis, S., 1996. Recent volcanism in the Siqueiros transform fault; picritic basalts and implications ffor MORB magma genesis. Earth Planet. Sci. Lett. 144, 91–108.

Pertermann, M., Hirschmann, M.M., Hametner, K., Günther, D., Schmidt, M.W., 2004. Experimental determination of trace element partitioning between garnet and silica-rich liquid during anhydrous partial melting of MORB-like eclogite. Geochem. Geophys. Geosyst. 5. doi:10.1029/2003GC000638. Q05A01.

Pringle, M.S., Frey, F.A., Mervine, E.M., 2008. A simple linear age progression for the Ninetyeast Ridge, Indian Ocean: new constraints on Indian plate tectonics and hotspot dynamics. Eos Trans. AGU Fall Meet. Suppl. Abstr. 89 (53), T54B-03.

Saunders, A.D., Storey, M., Gibson, I.L., Leat, P., Hergt, Thompson, R.N., 1991. Chemical and isotopic constraints on the origin of basalt from Ninetyeast Ridge: results from DSDP Legs 22 and 26 and ODP Leg 121, in Proc. ODP Sci. Res. 121, 559–590.

Thompson, G., Bryan, W.B., Frey, F.A., Sung, C.M., 1974. Petrology and geochemistry of basalts and related rocks from sites 214, 215, 216, DSDP Leg 22, Indian Ocean. Initial Reports of the Deep Sea Drilling Project, vol. 22. U.S. Government Printing Office, Washington, D.C, pp. 459–468.

Tuff, J., Gibson, S.A., 2007. Trace-element partitioning between garnet, clinopyroxene and Fe-rich picritic melts at 3 to7 GPa. Contrib. Mineral. Petrol 153, 369–387.

Van Westrenen, W., Draper, D.S., 2007. Quantifying garnet-melt trace element partitioning using lattice-strain theory: new crystal–chemical and thermodynamic constraints. Contrib. Mineral. Petrol. 154, 719–730.

Walter, M.J., 1998. Melting of garnet peridotite and the origin of komatite and depleted lithosphere. J. Petrol. 39, 29–60. doi:10.1093/petrology/39.1.29.

Weis, D., Frey, F.A., 1991. Isotope geochemistry of Ninetyeast Ridge basement basalts: Sr, Nd and Pb evidence for the involvement of the Kerguelen hotspot, in Proc. ODP Sci. Res. 121, 591–610.

Weis, D., Frey, F.A., Leyrit, H., Gautier, I., 1993. Kerguelen Archipelago revisited: geochemical and isotopic study of the Southeast Province lavas, Earth Planet. Sci. Letts. 118, 101–119.

Whitaker, E.J.W., Muntus, R., 1970. Ionic radii for use in geochemistry. Geochim. Cosmochim. Acta 34, 945–956.

Xu, G., Frey, F.A., Weis, D., Scoates, J.S., Giret, A., 2007. Flood basalts from Mt. Capitole in the central Kerguelen Archipelago: insights into the growth of the archipelago and source components contributing to plume-related volcanism. Geochem. Geophys. Geosyst. 8, Q06007. doi:10.1029/2007GC001608.

Yang, H.-J., Frey, F.A., Weis, D., Giret, A., Pyle, D., Michon, G., 1998. Petrogenesis of the flood basalts forming the northern Kerguelen Archipelago: implications for the Kerguelen Plume. J. Petrol. 39, 711–748.